

# Large-Scale Molecular Dynamics Simulations of Dislocation Intersection in Copper

S. J. Zhou,\* D. L. Preston, P. S. Lomdahl, D. M. Beazley

The results of massively parallel three-dimensional molecular dynamics simulations of the perpendicular intersection of extended dislocations in copper are reported. The intersection process, which involves three of the four possible  $\{111\}$  glide planes in the face-centered cubic lattice, begins with junction formation, followed by unzipping, partial dislocation bowing, cutting, and, finally, unit jog formation. The investigation provides insights into this complex atomistic process, which is currently not accessible to experimental investigation.

The resistance of a face-centered cubic (fcc) crystal to dislocation glide is less than  $10^{-5} \mu$  (1, 2), where  $\mu$  is the shear modulus. Forest intersection—that is, the intersection of mobile dislocations with dislocations on other glide planes—is therefore the principal mechanism limiting the glide of dislocations at low strain rates ( $10^{-6}$  to  $\sim 100 \text{ s}^{-1}$ ). Recent research (3) indicates that forest intersection also predominates in the regime of much higher strain rates, up to at least  $10^5 \text{ s}^{-1}$ . In fcc metals, such as copper, intersection processes are complex because dislocations are dissociated into two partial dislocations separated by a stacking fault; this combined structure is commonly referred to as an extended dislocation. There are a large number of potentially important intersection mechanisms. The intersection of attractive extended dislocations can lead to the formation of barriers that impede the motion of other dislocations. The most important examples are Lomer-Cottrell barriers (4) and Hirth dislocation locks (5). In contrast to attractive intersections, there has been no research on repulsive intersection processes.

There is no existing experimental technique that provides information on the intersection process itself; the intersection mechanism must be inferred. With transmission electron microscopy, for example, one observes only the jogs or kinks left behind after the intersection process is complete (6). Theoretical approaches are confronted by complexities on two length scales: the mutual bending and twisting of approaching dislocations over distances up to about  $1 \mu\text{m}$  as a result of their linear elastic interactions, and the interactions

between dislocation cores on an atomic scale. Static continuum elastic dislocation theory cannot be applied to the discrete dislocation core-core overlap region, and moreover, the static theory is inapplicable when the applied stresses are sufficiently high to drive the intersecting dislocations at an appreciable fraction of the sound velocity, where retardation (relativistic) effects are potentially important. Molecular dynamics (MD) naturally encompasses both the dislocation core-scale physics and retardation effects and is currently the only viable approach for investigating the intersection process. In principle, all types of dislocation intersection processes not involving slow processes such as diffusion can be investigated with MD. With the advent of massively parallel computers, calculations involving millions of atoms are now feasible (7, 8), allowing the simulation of the interactions between dislocation cores during the intersection process.

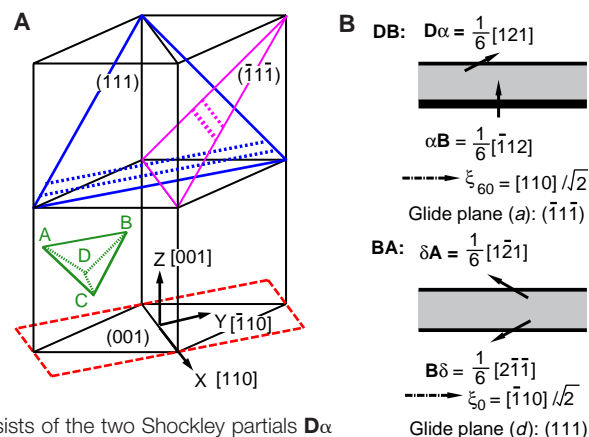
We have developed a MD code, SPaSM (Scaleable, Parallel, Short-Range Molecular Dynamics) (7), designed for efficiently computing and analyzing the huge amount of data generated in large-scale computer simulations in three di-

mensions. Here we report the results of a MD simulation of repulsive dislocation intersection in copper, a typical fcc metal with a low stacking-fault energy, revealing the intermediate stages that lead to jog formation.

The embedded-atom method (EAM) potential, a many-body form in which a pairwise interaction is augmented with a term that depends on the local atomic density (9, 10), provides a good description of fcc transition metals with completely empty or filled  $d$  bands, such as copper. Here we choose the copper EAM potential developed by Voter (10, 11), for which the lattice constant  $a_0 = 3.614 \text{ \AA}$  and the stacking-fault energy is  $0.0361 \text{ J/m}^2$ . Throughout this paper we measure Burgers vectors (dislocation-displacement vectors, equal to the line integral of the elastic displacement around the dislocation) in units of  $a_0$ . We use Thompson's well-known notation for glide planes and Burgers vectors in the fcc lattice (1).

We chose to investigate the intersection of perpendicular dislocations in order to minimize the sizes of junctions formed during the intersection process. Perpendicular intersection can occur only between dislocations parallel to the edges of the Thompson tetrahedron (Fig. 1A), that is, the regular tetrahedron with faces parallel to the close-packed  $\{111\}$  primary glide planes. All such edge pairs are equivalent, and therefore, the dislocations were placed, without loss of generality, on the  $d = (111)$  and  $a = (\bar{1}\bar{1}\bar{1})$  glide planes with sense vectors (unit tangent vectors to the dislocation line)  $[\bar{1}\bar{1}0]/\sqrt{2}$  and  $[110]/\sqrt{2}$ , respectively (Fig. 1A). The dislocation on the  $d$  plane was chosen to be a screw dislocation in order for it to remain stationary in a compressive stress field. Its Burgers vector was chosen to be  $\mathbf{BA} = \frac{1}{2}[\bar{1}\bar{1}0]$ . The Burgers vector of the other dislocation was chosen to be  $\mathbf{DB} = \frac{1}{2}[011]$  (12), so it was a  $60^\circ$

**Fig. 1. (A)** Schematic of the MD computational cell. The red dashed lines indicate the boundary of the computational cell; the dotted lines represent the perpendicular extended dislocations  $\mathbf{BA}$  and  $\mathbf{DB}$ . The stationary extended screw dislocation  $\mathbf{BA} = \frac{1}{2}[\bar{1}\bar{1}0]$  with sense vector  $\xi_0 = \hat{y}$  passes through the center of the computational cell on the  $d$  plane. The  $60^\circ$  dislocation  $\mathbf{DB} = \frac{1}{2}[011]$  has sense vector  $\xi_{60} = \hat{x}$  and lies on the  $a$  plane. Note the Thompson tetrahedron ABCD in green. **(B)** Structure of the extended dislocations. The  $60^\circ$  dislocation  $\mathbf{DB}$  with sense vector  $[110]/\sqrt{2}$  consists of the two Shockley partials  $\mathbf{D}\alpha$  and  $\alpha\mathbf{B}$  on the  $(\bar{1}\bar{1}\bar{1})$  glide plane. The screw dislocation  $\mathbf{BA}$  has sense vector  $[\bar{1}\bar{1}0]/\sqrt{2}$  and is dissociated into  $\mathbf{B}\delta$  and  $\delta\mathbf{A}$  on  $(111)$ .



S. J. Zhou and D. L. Preston, Applied Theoretical and Computational Physics Division, Los Alamos National Laboratory, Los Alamos, NM 87545, USA.  
 P. S. Lomdahl and D. M. Beazley, Theoretical Division, Los Alamos National Laboratory, Los Alamos, NM 87545, USA.

\*To whom correspondence should be addressed. E-mail: sjzhou@lanl.gov

mixed dislocation (a  $60^\circ$  angle between its Burgers vector and its sense vector). The interaction between  $\mathbf{DB}$  and  $\mathbf{BA}$  is repulsive according to the Peach-Koehler formula (1).

The computational cell was a parallelepiped containing 200,000 to 3.5 million atoms at an initial temperature of 0.01 K. Free boundary conditions were employed on all faces of the computational cell. We note that the unavoidable asymmetric emplacement of at least one of the two perpendicular dislocations precludes the imposition of periodic boundary conditions. Interactions between the dislocations and the free boundaries, resulting in image forces, have some effect on the intersection dynamics. However, the effects of image forces were minimized in our simulations by arranging for intersection to occur near the center of the computational cell, where the image forces nearly cancel.

Placement of the two perfect dislocations in the computational cell was achieved by displacing the atoms from their fcc lattice sites in accordance with isotropic linear elasticity theory (1). After placement of the dislocations, the system was allowed to relax for  $5 \times 10^{-13}$  s. During this time, the dislocations  $\mathbf{BA}$  and  $\mathbf{DB}$  dissociate into extended dislocations consisting of two Shockley partials separated by an intrinsic stacking fault (Figs. 1B and 2A). The initial screw  $\mathbf{BA}$  dissociates into  $\delta\mathbf{A}$  and  $\mathbf{B}\delta$ , each  $30^\circ$  partials;  $\mathbf{DB}$  dissociates into  $\alpha\mathbf{B}$ , an edge partial, and  $\mathbf{D}\alpha$ , another  $30^\circ$  partial. At  $5 \times 10^{-13}$  s, a homogeneous compressive elastic strain in the  $z$  direction only is imposed on the system at a constant elastic strain rate

until a predetermined value of the elastic strain  $\epsilon_{zz}$  is attained at time  $\tau$ . Subsequently,  $\epsilon_{zz}$  was maintained throughout the computational cell by permanently fixing the positions of the atoms in a few layers on the top and bottom of the cell at their locations at time  $\tau$ , but allowing all other atoms to move according to the equations of motion. Points where the partials exit the computational cell serve as weak pinning (more precisely dragging) points.

For the discussion that follows, it will prove convenient to define the outside (inside) of a glide plane as that half-space occupied by an observer on the outside (inside) of the Thompson tetrahedron. Under the applied compressive stress,  $\alpha\mathbf{B}$  glides toward the stationary screw  $\mathbf{BA}$ . Partial  $\alpha\mathbf{B}$  does not pass  $\delta\mathbf{A}$ , the leading screw partial, but instead forms a junction. Reaction of the partials to form a stair-rod junction with Burgers vector  $\alpha\delta/\mathbf{AB} = \frac{1}{6}[01\bar{3}]$  is energetically favored. After junction formation,  $\alpha\mathbf{B}$  remains nearly stationary on the inside of the  $d$  plane but continues to glide on the outside until it encounters the screw partial  $\mathbf{B}\delta$ . A stair-rod junction is formed along the intersection of the  $d$  and  $a$  planes by means of the reaction  $\alpha\mathbf{B} + \mathbf{B}\delta \rightarrow \alpha\delta$ , which is also favored energetically (Fig. 2B). Like  $\alpha\mathbf{B}$ ,  $\mathbf{B}\delta$  barely moves on the inside of the  $a$  plane, but  $\alpha\mathbf{B}$  and  $\mathbf{B}\delta$  continue to glide on the outsides of the  $d$  and  $a$  planes, respectively, thereby lengthening the  $\alpha\delta$  junction. The growth of this junction halts at a length of about  $7a_0$  and then unzips as the stacking fault in  $\mathbf{BA}$  contracts on the outside of the  $a$  plane. The edge partial  $\alpha\mathbf{B}$  bows asymmetrically around the now highly contracted screw (Fig. 2C). The

outside segment bows until it is roughly perpendicular to its original direction, whereas the inside segment bows to only about  $20^\circ$ . When the two segments meet at a critical breaking angle  $\phi_c = 70^\circ$ ,  $\alpha\mathbf{B}$  passes the screw and is left with a jog of length  $|\mathbf{BA}|$  with sense vector  $\mathbf{BA}/|\mathbf{BA}|$ . As  $\alpha\mathbf{B}$  continues to glide, an extended unit jog forms between the contracted screw and the jog in  $\alpha\mathbf{B}$  (Fig. 2D). The MD simulations show that the stair rods bounding the extended jog lie along the intersection of the  $a$  and  $c$  planes, that is, in the  $[01\bar{1}]$  direction; hence, the extended jog lies in the  $c$  plane. Partial  $\mathbf{D}\alpha$  is perturbed only locally (Fig. 2, D and E) when it interacts with the stair rods and the screw; no appreciable bowing occurs. When  $\mathbf{D}\alpha$  passes the screw dislocation, it acquires a unit jog with the same length and direction as the jog in  $\alpha\mathbf{B}$ , thus completing the formation of an extended unit jog (jog line) in the mixed dislocation with a width of approximately  $20a_0$ . The screw dislocation is left with a highly contracted unit jog (Fig. 2F). At the completion of the intersection process ( $1.2 \times 10^{-11}$  s), the angle between the segments of  $\alpha\mathbf{B}$  meeting at the jog line is  $100^\circ$ . This angle gradually increases to  $110^\circ$  at  $1.4 \times 10^{-11}$  s (Fig. 2F). In contrast, the segments of  $\mathbf{D}\alpha$  on both sides of the jog line are relatively straight and parallel. The velocity of  $\mathbf{D}\alpha$  was measured before and after intersection and was found to be unchanged. At the largest applied compressive elastic strain used in the simulations, namely, 0.04, the velocity of the partial  $\mathbf{D}\alpha$  is about  $0.4v_t$ , where  $v_t$  is the transverse sound speed in copper, so relativistic effects can be neglected.

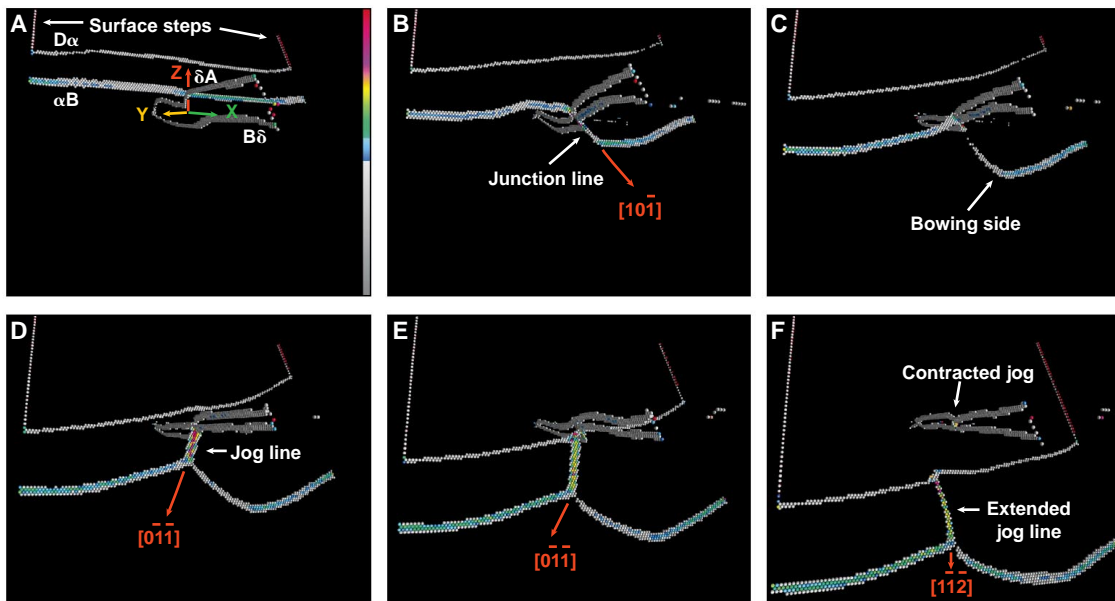


**Fig. 2.** The dislocation intersection process in copper at times (A)  $1.6 \times 10^{-12}$  s, (B)  $5.0 \times 10^{-12}$  s, (C)  $7.2 \times 10^{-12}$  s, (D)  $8.1 \times 10^{-12}$  s, (E)  $1.1 \times 10^{-11}$  s, and (F)  $1.4 \times 10^{-11}$  s. The computational cell has dimensions  $L_x = L_y = 85a_0$  and  $L_z = 120a_0$ . To visualize the dislocations, only atoms with potential energies between  $-3.49$  eV and  $-3.39$  eV are shown.

REFERENCES AND NOTES

1. J. P. Hirth and J. Lothe, *Theory of Dislocations* (Wiley, New York, 1982).
2. S. J. Zhou, A. E. Carlsson, R. Thomson, *Phys. Rev. B* **49**, 6451 (1994).
3. P. S. Follansbee and U. F. Kocks, *Acta Metall.* **36**, 81 (1988).
4. W. M. Lomer, *Philos. Mag.* **42**, 1327 (1951); A. H. Cottrell, *ibid.* **43**, 645 (1952).
5. J. P. Hirth, *J. Appl. Phys.* **32**, 700 (1961); J. P. Hirth, *ibid.* **33**, 2286 (1962); D. Kuhlman-Wilsdorf, *Acta Metall.* **14**, 439 (1966).
6. C. B. Carter and P. B. Hirsch, *Philos. Mag.* **35**, 1509 (1977).
7. P. S. Lomdahl, P. Tamayo, N. Gronbeck-Jensen, D. M. Beazley, *Proceedings of Supercomputing 93* (IEEE Computer Society Press, Los Alamitos, CA, 1993), pp. 520–527; D. M. Beazley and P. S. Lomdahl, *Parallel Comput.* **20**, 173 (1994).
8. S. J. Zhou, D. M. Beazley, P. S. Lomdahl, B. L. Holian, *Phys. Rev. Lett.* **78**, 479 (1997).
9. M. S. Daw, S. M. Foiles, M. I. Baskes, *Mater. Sci. Rep.* **9**, 251 (1995).
10. The EAM assumes that the energy of a solid consists of an electrostatic pair interaction plus an embedding energy, which can be written as
 
$$E_{\text{tot}} = \sum_i F_i(\rho_{n,i}) + \frac{1}{2} \sum_i \sum_{j \neq i} \Phi_{ij}(R_{ij}) \quad (2)$$
 where  $F_i(\rho_{n,i})$  is the energy to embed atom  $i$  into the background electron density  $\rho_{n,i}$ , and  $\Phi_{ij}(R_{ij})$  is the classical electrostatic interaction between atoms  $i$  and  $j$ , separated by the distance  $R_{ij}$ . Electron density  $\rho_{n,i}$  is approximated by  $\sum_{j \neq i} \rho_j(R_{ij})$ , where  $\rho_j$  is the electron density contributed by atom  $j$ . The copper EAM potential can describe grain-boundary structures well [J. Wolf, F. Ernst, T. Muschik, M. W. Finis, H. F. Fischmeister, *Philos. Mag. A* **66**, 991 (1992)], although calculated defect energies are not very accurate (9). The copper potential used here was fit to the bulk lattice constant, cohesive energy, elastic constants, and vacancy formation energy, as well as the bond energy and bond length of the gas-phase copper dimer.
11. A. F. Voter, *Los Alamos National Laboratory Unclassified Technical Report LA-UR-93-3901* (1993); in *Intermetallic Compounds: Principles and Practice*, J. H. Westbrook and R. L. Fleischer, Eds. (Wiley, New York, 1995), vol. 1, p. 77.
12. There are six choices for the Burgers vector of the dislocation on the  $a$  plane:  $\pm \frac{1}{2}[110]$ ,  $\pm \frac{1}{2}[011]$ , and  $\pm \frac{1}{2}[\bar{1}01]$ . The vectors  $\pm \frac{1}{2}[110]$  are uninteresting because, like **BA**, they are screw dislocations and would also not move under compression. Of the four remaining choices, all  $60^\circ$  mixed dislocations, we chose arbitrarily the case **DB** =  $\frac{1}{2}[011]$  for this investigation.
13. C. B. Carter, *Phys. Status Solidi A* **54**, 395 (1979).
14. K. H. Pfeffer, P. Schiller, A. Seeger, *Phys. Stat. Solidi* **8**, 517 (1965).
15. B. Devincere and L. P. Kubin, *Model. Simul. Mat. Sci. Eng.* **2**, 559 (1994).
16. A. Kelley and R. B. Nicholson, *Strengthening Methods in Crystals* (Wiley, New York, 1971); A. J. E. Foreman, *Acta Metall.* **3**, 322 (1955).
17. M. A. Meyers, *Dynamic Behavior of Materials* (Wiley, New York, 1994).
18. H. M. Zbib, M. Rhee, J. P. Hirth, in *Advances in Engineering Plasticity and Its Applications*, T. Abe and T. Tsuta, Eds. (Pergamon, Oxford, 1996), pp. 15–20.
19. Computations were performed at Los Alamos National Laboratory on the Cray T3D at the Advanced Computing Laboratory and on a SUN Enterprise 4000 in the Theoretical Division. We acknowledge helpful discussions with J. Hirth, G. Schoeck, R. deWit, B. Holian, R. Hoagland, F. Louchet, R. Thomson, M. Verdier, S. Yip, and V. Vitek.

30 September 1997; accepted 29 January 1998

With the weak-beam technique of electron microscopy, Carter (13) observed in copper doped with 15.8% aluminum (stacking fault energy,  $0.004 \text{ J/m}^2$ ) contracted and extended jogs and concluded that the extension of a jog depends on several factors, including the height of the jog and the character of the dislocation. However, a detailed characterization of the final configuration was beyond his experimental resolution. Here the jog line on the mixed dislocation is not fully contracted, whereas that on the screw dislocation is, or is nearly so; thus, the overall results are consistent with Carter's.

The extended jog is obtuse (Fig. 3), and therefore, the Shockley partials bounding the jog must be viewed from within the Thompson tetrahedron. The climb or glide of an isolated stair rod leads to the formation of a high-energy stacking fault. Consequently, the jog line is expected to move parallel to the stair rods, that is, in the  $[0\bar{1}1]$  direction. This prediction is approximately true in our simulations during (Fig. 2D) and immediately after intersection (Fig. 2E), but a deviation from  $[0\bar{1}1]$  to  $[1\bar{1}2]$  is observed as the unit jog continues to move away (Fig. 2F). Pfeffer *et al.* (14) pointed out that jog lines lying along  $\langle 112 \rangle$  directions are energetically possible. Deviations of jog lines from the  $\langle 011 \rangle$  to the  $\langle 112 \rangle$  directions have been observed (13), although the fine structure of the deviated jog lines cannot be resolved experimentally. The motion of the jog line is nonconservative, so existing dislocation theory (1) would suggest that vacancies or interstitials are formed behind the moving jog line. However, no vacancies or interstitials were observed in our simulations after a search of the entire range of atomic potential energies. The reason for this is likely to be the fact that the stair rods are only separated by one lattice spacing, so that their glide plane is not well defined, and therefore, the jog line can move freely like a perfect screw dislocation.

The critical breaking angle  $\phi_c$  determines the evolution of dislocation microstructures, but no accurate values of this

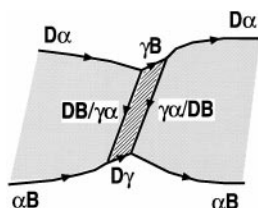


**Fig. 3.** Schematic of the obtuse extended unit jog in the mixed dislocation. The shaded stacking fault lies on  $a = (\bar{1}1\bar{1})$ , and the jog (hatched) is on  $c = (111)$ . Stair-rod dislocations  $\pm \text{DB}/\gamma\alpha$  lie along the intersection of  $(\bar{1}1\bar{1})$  and  $(111)$ .

fundamental parameter are available. The best estimate to date is that of Devincere and Kubin (15) for copper. They used the results of accurate measurements on single-crystal copper to determine that  $\phi_c$  lies between  $65^\circ$  and  $78^\circ$ , in good agreement with the present simulations.

The MD simulations show that **DB** can pass **AB** once the mounting stress on **AB** that results from the asymmetric bowing of  $\alpha\text{B}$  reaches a critical value; the trailing partial **D** $\alpha$  easily passes through the extended dislocation. The critical stress  $\tau_c$  at which  $\alpha\text{B}$  cuts through **AB** can be estimated from the measured breaking angle. We use the fixed-tension formula (16)

$$\tau_c = \frac{\mu b}{2\pi L} \left( \frac{1 - \nu/2}{1 - \nu} \right) \ln \left( \frac{L}{b} \right) \cos \left( \frac{\phi_c}{2} \right) \quad (1)$$

to obtain an order-of-magnitude estimate of  $\tau_c$ . Here,  $b$  is the magnitude of the Burgers vector,  $\nu$  is the Poisson ratio, and  $L$  is the distance between two pinning obstacles. We approximate  $L$  with  $L_x$  and set  $\nu = 0.324$ . This formula assumes symmetric bowing of the dislocation segments around the obstacle (the contracted screw dislocation in the present case) and ignores the change in the character (edge or screw) of the dislocation along the bowed segments. Furthermore, this expression does not account for inertial or retardation effects. In a system with  $L_x = 42a_0$ , we find  $\tau_c = 0.0073\mu = 398 \text{ MPa}$ , which corresponds to an applied compressive elastic strain of 0.005.

An alternative estimate of  $\tau_c$  can be obtained by determining the applied compressive elastic strain for which the intersection time—that is, the time from first contact of the edge partial with the screw dislocation until jog formation is complete—is infinite. In a system with  $L_x = L_y = 42a_0$  and  $L_z = 120a_0$ , the intersection time approaches infinity at a compressive strain of about 0.005, in agreement with our rough estimate based on Eq. 1. The intersection time decreases rapidly with increasing applied stress because of both an increase in the mean glide velocity of **DB** and a decrease in the width of **BA**.

The dislocation intersection process is unchanged by variations in the loading stress from 395 MPa to 3.17 GPa, or by changes in the system size from 200,000 to 3.5 million atoms. The MD simulations presented here allow the construction of simple analytic models that accurately represent the intersection process, essential input for the development of constitutive models (17) and for numerical simulations of a three-dimensional discrete system of dislocations (15, 18).